We are IntechOpen,
the world's leading publisher of Open Access books
Built by scientists, for scientists

6,900
Open access books available

185,000
International authors and editors

200M
Downloads

154
Countries delivered to

Our authors are among the

TOP 1%
most cited scientists

12.2%
Contributors from top 500 universities

CLARIVATE ANALYTICS

BOOK CITATION INDEX

INDEXED

WEB OF SCIENCE™

Selection of our books indexed in the Book Citation Index
in Web of Science™ Core Collection (BKCI)

Interested in publishing with us?
Contact book.department@intechopen.com

Numbers displayed above are based on latest data collected.
For more information visit www.intechopen.com

Magneto-optical Devices for Optical Integrated Circuits

Vadym Zayets and Koji Ando
Nanoelectronics Research Institute, National Institute of
Advanced Industrial Science and Technology (AIST)
Japan

1. Introduction

Magneto-optical materials have two unique properties, which make them important for a variety of optical applications. The first property is non-reciprocity. The time inverse symmetry is broken in magneto-optical materials. Therefore, properties of magneto-optical materials are different for two opposite directions of light propagation and optical non-reciprocal devices like the optical isolator and the optical circulator can be fabricated only by utilizing magneto-optical materials. The second important property of the magneto-optical materials is a memory function. If the material is ferromagnetic, the data can be memorized by means of two opposite directions of the residual magnetization. Both the reading and writing of such memory can be done by magneto-optical effect.

The optical isolator is an important component of optical networks. It is transparent in one direction and blocks light in opposite direction. Due to the imperfect matching between optical components in the network, the unwanted back reflection always exists and it severely disturbs the network performance. To avoid this, the optical components have to be protected by an optical isolator. Also, the isolator is important to cut the back-travelling amplified spontaneous emission in the case of serially-connected amplifiers.

Today there is a big demand to integrate all optical components into an opto-electronics chip. In fact, the isolator is one of few components, which have not yet been integrated into commercial chips. It is because of difficulties to integrate magneto-optical materials into a semiconductor-made chip. To solve this, we proposed to use (Cd,Mn)Te as a magneto-optical material for such isolator. The (Cd,Mn)Te exhibits a huge Faraday effect and can be grown on a semiconductor substrate. For (Cd,Mn)Te waveguide grown on GaAs substrate we achieved a high Faraday rotation of 2000 deg/cm, a high isolation ratio of 27 dB, a low optical loss of 0.5 dB/cm, and a high magneto-optical figure-of-merit of 2000 deg/dB/kG in a wide 25-nm wavelength range (Debnath et al., 2007). These values meet or exceed similar values of commercial discrete isolators.

We predicted theoretically (Zaets & Ando, 1999) and proved experimentally (Zayets & Ando, 2005) the effect of non-reciprocal loss in hybrid semiconductor/ferromagnetic metal waveguides. This effect can be utilized for new designs of waveguide optical isolator. Because the structure of this isolator is similar to that of laser diode, such a design is beneficial for the integration. The bistable laser diode with non-reciprocal amplifier was proposed to be used for high-speed optical logic (Zayets & Ando, 2001).

We proposed the non-volatile high-speed optical memory, which utilizes the magnetization reversal of nanomagnet by spin-polarized photo-excited electrons. It was demonstrated experimentally that one selected pulse from a train of two optical data pulses with interval of 450 fs can solely excite the spin-polarized electrons without a disturbance from the unselected optical data pulse (Zayets & Ando, 2009). This proves feasibility for proposed memory to record data train with rate of 2.2 TBit/sec.

2. $Cd_{1-x}Mn_xTe$ waveguide optical isolator

The conventional bulk-type optical isolator consists of a 45-degree Faraday rotator placed between two polarizers [Fig.1]. The angle between axes of entrance polarizer and exit polarizer is 45 degrees. In forward direction the polarization of light is 45 degree rotated by the Faraday rotator to be along the axis of the exit polarizer. Therefore, the light can pass through the isolator in forward direction. In backward direction, the direction of polarization rotation is opposite to that in forward direction due the non-reciprocal nature of the magneto-optical effect. At the entrance polarizer, the polarization is 90 degrees to the polarizer axis and the light is fully blocked.
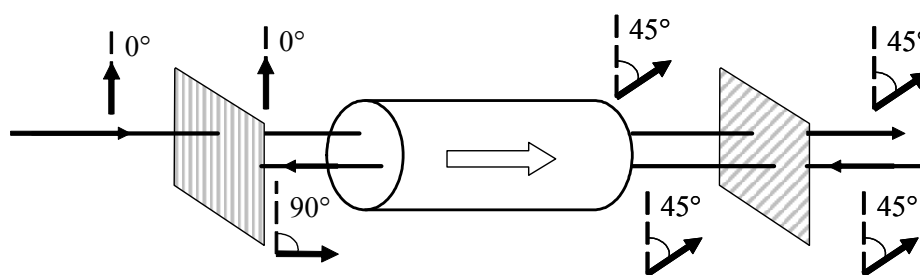

Fig. 1. Design of free-space optical isolator. The Faraday rotator is placed between entrance polarizer (left side) and exit polarizer (right side). Upper diagrams show polarization in forward direction. Lower diagrams show polarization in backward direction.

In present optical networks, ferrimagnetic garnet oxide crystals such as $Y_3Fe_5O_{12}$ (YIG) and $(GdBi)_3Fe_5O_b$ are used as magneto-optical materials for discrete optical isolators. Because most of the active optical elements (such as the laser diode, optical amplifier, modulator, and optical gate) are produced on GaAs or InP substrates, it is desirable to integrate monolithically all optical components on these types of substrate, but integration of the isolator is a difficult task. Waveguide optical isolator based on the garnet film has been reported (Ando et al., 1988). But the garnet-made isolators have not been monolithically integrated with semiconductor optoelectronic devices, because these oxide crystals can not be grown on semiconductor substrates.

Paramagnetic semiconductor $Cd_{1-x}Mn_xTe$ is promising as a magneto-optical material for integrated optical isolators and circulators. $Cd_{1-x}Mn_xTe$ shares the zinc-blende crystal structure with the typical semiconductor optoelectronic materials such as GaAs and InP; thus its film can be grown directly on GaAs and InP substrates. $Cd_{1-x}Mn_xTe$ also exhibits a huge Faraday effect (its Verdet constant is typically 50-200 deg/cm/kG) (Furdyna 1988) near its absorption edge because of the anomalously strong exchange interaction between the sp-band electrons and the localized d-electrons of Mn^{2+}. Furthermore, the tunability of its absorption edge from 1.56 to 2.1 eV with Mn concentration makes the $Cd_{1-x}Mn_xTe$ magneto-optical waveguide compatible with (Al,Ga,In)P:GaAs optoelectronic devices operating in the wavelength range of 600-800 nm. For longer-wavelength (λ=800-1600 nm)

optoelectronic devices, $Cd_{1-x-y}Mn_xHg_yTe$ can be used. Bulk optical isolators using these materials are now commercially available (Onodera et al. 1994).
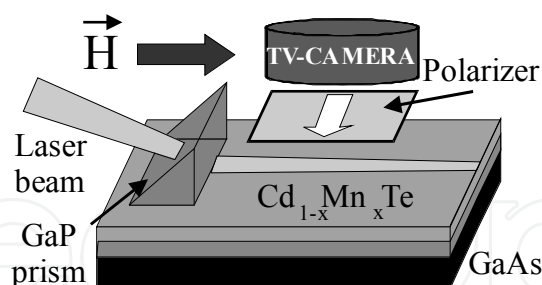

Fig. 2. Experimental set-up to evaluate magneto-optical TE-TM waveguide mode conversion

For the $Cd_{1-x}Mn_xTe$ to be used as a material for the waveguide isolator, several conditions should be satisfied. For a practical $Cd_{1-x}Mn_xTe$ waveguide isolator, the isolation ratio should exceed 20 dB, insertion loss should be below 1 dB and operation wavelength range should be wider than 20 nm. This performance can only be achieved with a magneto-optical waveguide having a mode conversion ratio above 95 % and a figure-of-merit above 100 deg/dB. Below we will show that using advanced waveguide structure and optimized fabrication technique, this conditions can be achieved in $Cd_{1-x}Mn_xTe$ waveguide grown on GaAs substrate.

The $Cd_{1-x}Mn_xTe$ has about 12% lattice mismatch with GaAs. The growth conditions of $Cd_{1-x}Mn_xTe$ on GaAs substrate should be well optimized. Otherwise, the high density of dislocation in $Cd_{1-x}Mn_xTe$ film causes high optical loss in $Cd_{1-x}Mn_xTe$ waveguide (Zaets et al.,1997) and low value of Faraday rotation. The $Cd_{1-x}Mn_xTe$ waveguide was grown by molecular beam epitaxy (MBE) on GaAs (001) substrate. We optimized the growth conditions and fabricated the $Cd_{1-x}Mn_xTe$ waveguide in the following way. In the beginning, GaAs substrate was thermally cleaned at 400^0 C under atomic hydrogen flux to remove oxides from GaAs surface. Before initiating the growth, the GaAs substrate was kept for 30 minutes under Zn flux to prevent the formation of the undesired Ga_2Te_3 compound. At first, a thin 10 nm ZnTe film was grown on the GaAs substrate to initialize the (001) growth. Following a 1-µm thick CdTe buffer layer, $Cd_{1-x}Mn_xTe$ waveguide was grown. It consists of a 3-µm-thick $Cd_{0.73}Mn_{0.27}Te$ waveguide cladding and a 1-µm-thick $Cd_{0.77}Mn_{0.23}Te$ waveguide core. The waveguide core was sandwiched between two 500-nm-thick $Cd_{1-x}Mn_xTe$ (x=0.27-0.23) graded-refractive-index clad layers, for which the Mn concentration was changed linearly with thickness. We used the $Cd_{0.73}Mn_{0.27}Te$ layer as a cladding layer, since GaAs is an optical absorber with a higher refractive index than that of $Cd_{1-x}Mn_xTe$, a single $Cd_{1-x}Mn_xTe$ layer on GaAs does not work as a waveguide. One needs transparent cladding layers with smaller refractive index. $Cd_{0.73}Mn_{0.27}Te$ satisfies these conditions because $Cd_{1-x}Mn_xTe$ with higher Mn concentration has a smaller refractive index and wider optical band gap. The graded-refractive-index clad layers are essential for $Cd_{1-x}Mn_xTe$ waveguide to achieve high magneto-optical TE-TM waveguide mode conversion and high optical isolation.

Figure 2 illustrates the experimental setup for evaluating optical propagation loss and TE-TM waveguide mode conversion (Zaets & Ando, 2000). A GaP prism was used to couple the laser light from tunable Ti:sapphire laser (λ=680 -800 nm) into a $Cd_{1-x}Mn_xTe$ waveguide. A cooled CCD TV-camera collected light scattered normally from the film surface. A linear polarizer was placed in front of the TV camera with its polarization axis perpendicular to

the light propagation direction. With this configuration, only the TE mode component of waveguiding light can be detected by the high-sensitivity TV camera. In the absence of a magnetic field, a scattered light streak was seen when the TE mode was excited (Fig. 3(a)), but it was not seen when TM mode was excited (Fig. 3 (b)). Also, weak dot-like scattering on defects was seen in both cases.
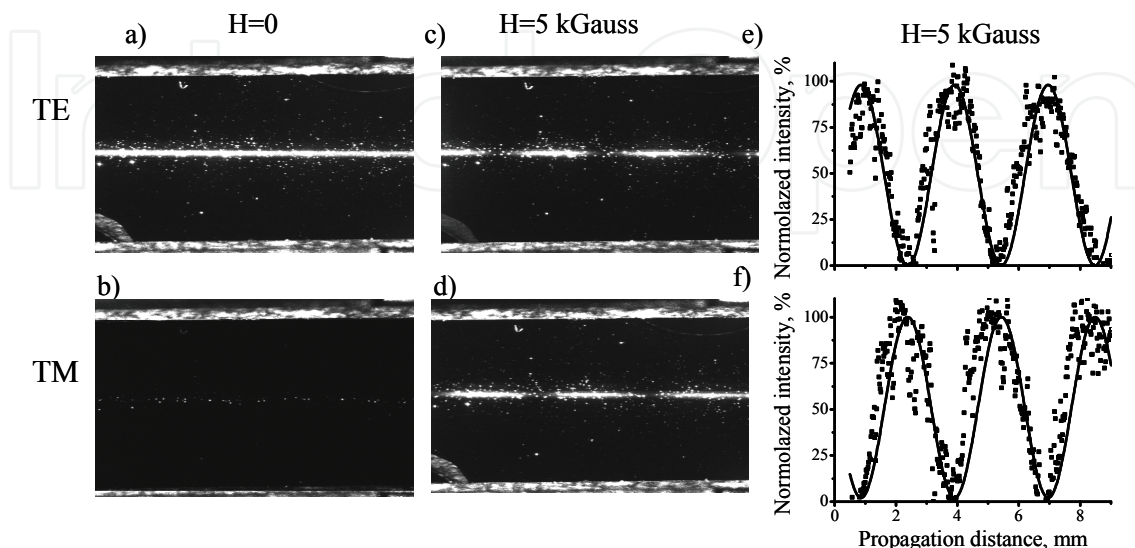

Fig. 3. TM-TE mode conversion ratio in $Cd_{1-x}Mn_xTe$ waveguide at λ=730 nm. (Zayets & Ando, 2004)

For the evaluation of the magneto-optical TE-TM waveguide mode conversion, a magnetic field was applied in parallel to the light propagation direction. A light streak with a periodically modulated intensity was observed for both TE mode excitation (Fig. 3 (c)) and TM mode excitation (Fig. 3 (d)). Figures 3 (e)-(f) show the measured intensity of the modulated streak along the propagation length. The intensity was normalized to input intensity. The oscillations maxima in the case of TE excitation (Fig. 3 (e)) correspond to the oscillations minima in the case of TM excitation (Fig. 3 (f)) and vice versa. Under an applied magnetic field the polarization of the waveguide mode rotates because of Faraday effect. If the TE-TM mode phase mismatch is not zero, the eigenmodes of the waveguide are elliptically polarized and the rotation between TE and TM polarizations is not complete. As seen from Figs. 3 (c)- 3 (f), the $Cd_{1-x}Mn_xTe$ waveguide with the graded index cladding layer shows almost complete mode conversion.

The $Cd_{1-x}Mn_xTe$ waveguide with graded buffer layers has low optical loss, high TE-TM mode conversion efficiency (more than 98 %) and high isolation ratio (more than 20 dB). However, high isolation ratio was obtained in narrow about 3 nm wavelength range. For practical application of the isolator the operation wavelength range should be at least 20 nm. For the operation of the optical isolator, the rotational angle of Faraday rotator should be 45^0 (Fig.1) for any operational wavelength. $Cd_{1-x}Mn_xTe$ is a diluted magnetic semiconductor. It has a high value of Faraday rotation, but it is high only near its bandgap and near the bandgap the dispersion of Faraday rotation is significant as well. Of course, $Cd_{1-x}Mn_xTe$ is a paramagnetic material and at each wavelength the Faraday rotation can be tuned to 45^0 by the changing magnetic field. However, such tuning is not practical for real applications because a practical isolator needs a permanent magnet with a fixed magnetic field. Below we will show that it is possible to achieve practically dispersion-free Faraday rotation in

wide wavelength range by combining in a waveguide $Cd_{1-x}Mn_xTe$ bulk material and a $Cd_{1-x}Mn_xTe$ quantum well (QW).

The Faraday effect in a $Cd_{1-x}Mn_xTe$ QW is greater than that of bulk $Cd_{1-x}Mn_xTe$ and it is not as dependent on wavelength. However, due to the two-dimensional nature of the QW, its optical properties become significantly different for light polarized in the plane of the QW and perpendicular to the QW. Therefore, for a waveguide composed of only a single QW, there is a big difference between propagation constants of TE and TM modes. Due to TE-TM mode phase mismatch, the linearly polarized light can be easily converted to elliptically polarized light, which reduces the performance of the isolator. Therefore, a waveguide composed of only a single QW cannot be used for the isolator application.

In order to make a high performance isolator, we need a large, wavelength independent Faraday effect and small phase mismatch between TE and TM modes. For that purpose, we proposed using an optical waveguide that combines $Cd_{1-x}Mn_xTe$ bulk material and a single QW (Debnath et.al. 2004)

Figure 4 shows the (Cd,Mn)Te/(Cd,Zn)Te QW waveguide structure. There are two buffer layers of ZnTe (10 nm) and CdTe (1 µm) and a $Cd_{0.71}Mn_{0.29}Te$ (3 µm) waveguide clad layer. The waveguide core layer was sandwiched between two $Cd_{1-x}Mn_xTe$ (0.5 µm) graded layers in order to reduce TE-TM mode phase mismatch. The waveguide core consists of a $Cd_{0.76}Mn_{0.2}Te/Cd_{0.75}Zn_{0.25}$ Te single QW and a 1-µm-thick $Cd_{0.75}Mn_{0.25}Te$ layer, where thickness of the $Cd_{0.76}Mn_{0.24}Te$ well varies between 20–100 Å and the thickness of $Cd_{0.75}Zn_{0.25}Te$ barrier is 100 Å.

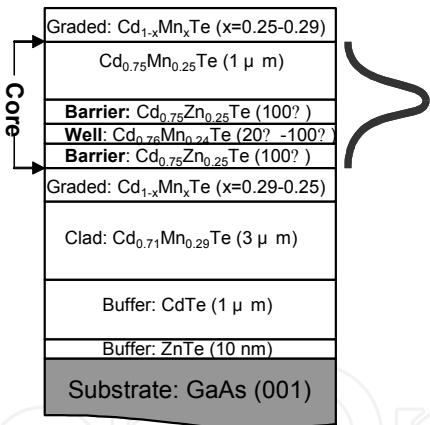Fig. 4. Structure of a (Cd,Mn)Te waveguide with (Cd,Mn)Te/(Cd,Zn)Te QW. The waveguiding light intensity distribution is shown in the right side . (Debnath et al, 2007)

Figure 5 shows a spatially modulated light streak of the waveguide mode at two different wavelengths (760 and 785 nm) for the waveguides with QW and without QW. The high contrast between the minima and maxima of the light intensity oscillations shows that complete mode conversion is attained for both waveguides. The distance between peaks corresponds to 180 degrees of the rotation. For the waveguide without QW [Figs. 5 (c) and 5 (d)], there is a big difference of the rotational period for these two wavelengths. However, for the waveguide with QW [Figs. 5(a) and 5 (b)], there was no such difference. This means that, for the waveguide with QW, the Faraday rotation at these two wavelengths is the same. Also, for the waveguide with QW, the oscillation period is much shorter than that of

the waveguide without QW. This corresponds to the larger Faraday rotation in the waveguide with QW.
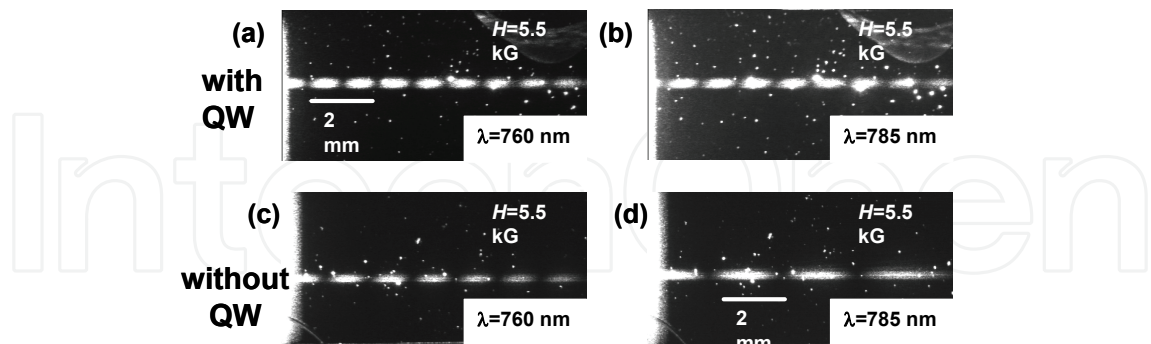

Fig. 5. Spatially modulated light streak from waveguide TE mode for CdMnTe waveguide with QW (a), (b) and waveguide without QW (c), (d) at λ = 760 nm (a), (c) and λ = 785 nm (b), (d) under magnetic field of 5.5 kG . (Debnath et al, 2007)

Figure 6 compares the Faraday effect in $Cd_{1-x}Mn_xTe$ waveguide with QW and without QW at H=5.5 kG. In the case of the waveguide with QW, the Faraday rotation is very high (~1800 deg/cm) and it is almost constant in a wide wavelength range. Figure 7 shows the wavelength range within which more than 95% conversion efficiency was obtained for the waveguide with single QW as a function of well width. For well widths of 20–40 Å, the operational wavelength range is as wide as 25-nm. However, for thicker well widths of 70–100 Å, the operational wavelength range sharply decreases. Analysis shows that the expansion of the wavelength range for thinner QW waveguides was due to the reduction of the mode phase mismatch, to as low as 50 deg/cm, whereas this value rose to more than 500 deg/cm for thicker QW waveguides. Thinner QW waveguides have high Faraday rotation (≈ 2000 deg/cm) and small phase mismatch (≈ 50 deg/cm) This is the reason why thinner QW waveguides provided a wider operational wavelength range of complete mode conversion. From this result we conclude that, for the practical optical isolator application, only waveguides with a single QW thinner than 40 Å can be used.
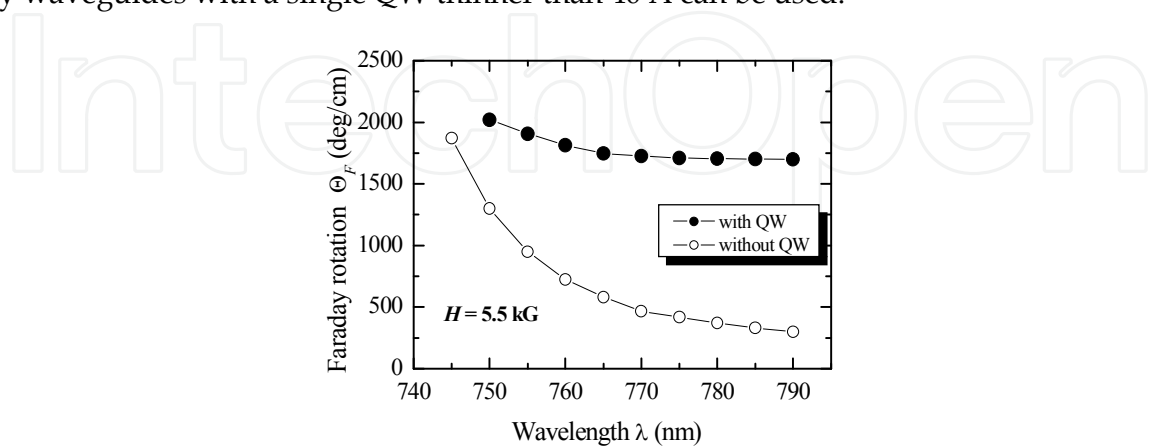

Fig. 6. Faraday rotation in $Cd_{1-x}Mn_xTe$ waveguide with QW and without QW . (Debnath et al, 2007)
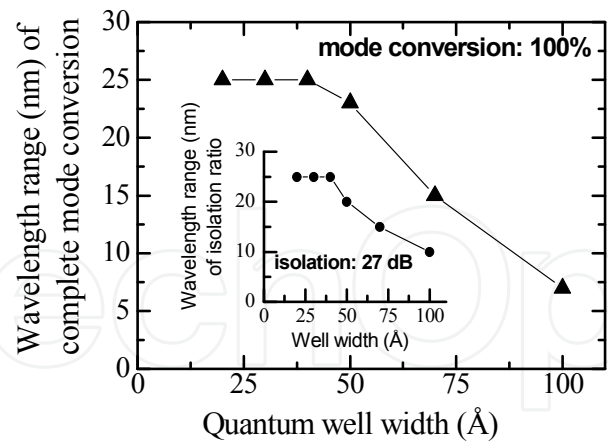
Fig. 7. Wavelength range, within which the complete mode conversion is obtained, as a function of QW width. Inset shows the isolation ratio. (Debnath et al, 2004)

For an integrated optical isolator, the CdMnTe magneto-optical waveguide has to be integrated with a reciprocal polarization rotator and a polarizing beam splitter. Both these components can be fabricated utilizing passive optical waveguides. The material of the waveguides is not essential for the operation of these components. Therefore, it is better to use the same passive waveguides as utilized for optical interconnection in a photonic circuit, where the isolator should be integrated. Figure 8 shows an example of a waveguide-type reciprocal polarization rotator. It is a passive optical waveguide in which the top is cut at an angle of 45 degrees. TM and TE modes are not eigenmodes in this waveguide. Therefore, there is a conversion between TM and TE mode along mode propagation. The length of this waveguide can be adjusted to achieve the desirable angle of polarization rotation. The waveguide type reciprocal polarization rotators were demonstrated utilizing Si waveguide (Brooks et al., 2006], AlGaAs waveguides (Huang et al., 2000) and GaInAsP/InP waveguides (Kim et al., 2009). Figure 11 shows an example of a waveguide-type polarizing beam splitter. It is a 2x2 waveguide splitter. In any waveguide splitter, the coupling efficiency between an input ports and an output ports depends on the value of mode propagation constant. Generally, in an optical waveguide the propagation constants of TM and TE modes are different. Therefore, it is possible to adjust the splitter so that the TM mode couples from port 1 into port 4 and the TE mode couples from port 1 into port 3. The waveguide-type polarizing beam splitters were demonstrated utilizing Si waveguide (Fukuda et al., 2006) and InGaAsP–InP waveguides (Augustin et al., 2007).
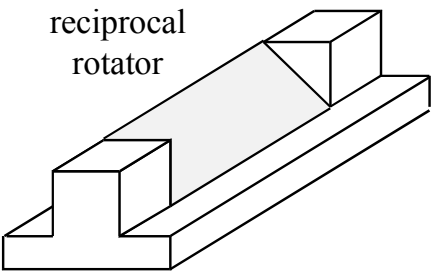

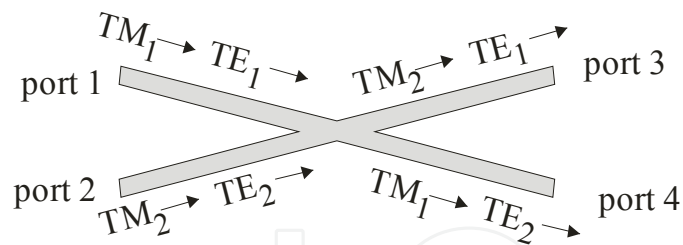Fig. 8. Waveguide-type reciprocal polarization rotator.

Fig. 9. Waveguide-type polarization beam splitter.

Figure 10 shows the design of a waveguide-type polarization-independent optical isolator. It consists of two polarizing beam splitters connected by two arms. Each arm consists of an 45-degree reciprocal rotator and a 45-degree $Cd_{1-x}Mn_xTe$ -made Faraday rotator. There is an optical absorber at port 2 to absorb backward travelling light. In the forward direction, the direction of polarization rotation in the Faraday rotator is the same as that in the reciprocal rotator and the total rotation angle by the reciprocal rotator and the Faraday rotator is 90 degrees. The light of both polarizations propagates through the isolator from input 1 port to output port 3. In the backward direction, the direction of polarization rotation in the Faraday rotator is opposite to that in the reciprocal rotator due to the non-reciprocal nature of the Faraday rotator. In this case, the total rotation angle is zero. The light propagates from output port 3 to the port 2, where there is an absorber. Therefore, the input port 1 is isolated. The optical paths for each polarization are shown in Fig. 10. A waveguide-type polarization-independent optical circulator can be fabricated utilizing the same design. In this case the correspondence between the input and output ports is: port 1-> port 3, port 2 –>port 4, port 3 -> port 2, port 4 -> port 1.
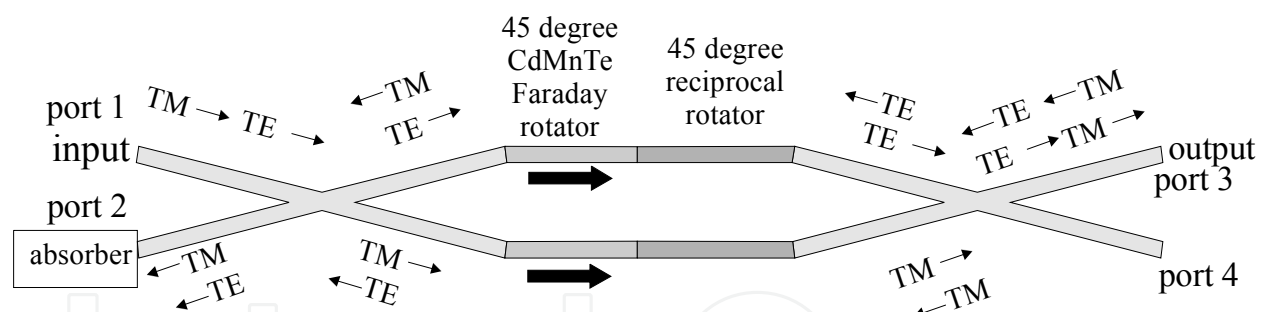

Fig. 10. Polarization-independent waveguide-type optical isolator / circulator. Polarization transformations for both propagation directions are shown.

In conclusion, the high performance of $Cd_{1-x}Mn_xTe$ waveguide isolator grown on GaAs substrate was demonstrated. Complete TE-TM mode conversion, a high Faraday rotation of 2000 deg/cm, a high isolation ratio of 27 dB, a low optical loss of 0.5 dB/cm, and a high magneto-optical figure-of-merit of 2000 deg/dB/kG were achieved in a wide 25-nm wavelength range. These values are comparable or better to that of commercial discrete isolators. The propagation of waveguide mode in $Cd_{1-x}Mn_xTe$ waveguide is very similar to the light propagation in magneto-optical bulk media. Therefore, non-reciprocal elements such as an optical isolator, circulator and polarization independent isolator can be fabricated by $Cd_{1-x}Mn_xTe$ waveguides using a similar scheme as is used for free space components. Therefore, using $Cd_{1-x}Mn_xTe$ all these components can be integrated with semiconductors optoelectronical components.

3. Ferromagnetic metal/semiconductor hybrid isolator

Both types of isolators, either made of $Cd_{1-x}Mn_xTe$ or made of garnets, required high-crystal quality materials in order to have a low optical loss and a high value of Faraday rotation. In the case of $Cd_{1-x}Mn_xTe$, the magneto-optical film can be directly grown on a semiconductor substrate. The defect density in $Cd_{1-x}Mn_xTe$ film should be kept low until the end of the microfabrication process. For the fabrication of integrated optical circuits it is more convenient to use common fabrication technique like sputtering, e-beam evaporation and lift-off. Ferromagnetic metals, like Fe, Co or Ni are very attractive for this purpose. They have high magneto-optical constants and the microfabrication of these metals is simple and well established for optoelectronic integrated circuits. For example, Cr and Co is often used as a metal for Ohmic contact to p-GaAs and p-InGaAs.

We predicted theoretically (Zaets & Ando, 1999) and proved experimentally (Zaets & Ando, 2005) the effect of non-reciprocal loss in hybrid semiconductor/ferromagnetic metal waveguides. This effect can be use for a new design of waveguide optical isolator. For this design, the magnetization of the ferromagnetic metal was perpendicular to the light propagation direction and lay in the film plane (Voigt configuration). In this case a large difference exists in values of loss/gain for TM modes propagating in opposite directions. Thus, an amplifier covered by a ferromagnetic metal can itself function as an optical isolator. This ferromagnetic-metal/ semiconductor hybrid isolator can be beneficial for monolithic integration of the optical isolator with semiconductor optoelectronic devices, because its structure is very similar to the structure of a laser diode and its fabrication process is almost the same as that of a laser diode. Therefore, the isolator can be integrated utilizing the present technology for a semiconductor laser diode and a semiconductor amplifier.

The effect of the non-reciprocal loss is unique for the hybrid waveguides. In the case of the light propagation in a bulk MO material the non-reciprocal effect (variation of optical properties for opposite directions of light propagation) occurs only when the magnetization of the material is parallel to the light propagation (Faraday effect and magnetic circular dichroism). There is no non-reciprocal effect, if the light propagates perpendicularly to the magnetization. On the contrary, in a MO waveguide, even if the magnetization is perpendicular to the light propagation direction and lies in the film plane, the TM mode has a non-reciprocal change of the propagation constant.

Figure 11 compares the magneto-optical effect in a bulk material and in an optical waveguide covered by ferromagnetic metal. In the bulk material, when the light propagates along magnetic field, there are two magneto-optical effects: magnetic circular dichroism (MCD) and Faraday effect. In magnetic materials the spin-up and spin-down bands are split along the magnetic field. Due to the conservation law of the time inverse symmetry, the light of the left circular polarization interacts only with the spin-up band and the light of the right circular polarization interacts only with the spin-down band. (In general, the light of elliptical polarization interacts solely with one spin band). Therefore, there is a difference of refractive index (Faraday effect) and of absorption (MCD effect) for the left and right circular polarizations, when the light propagates along the magnetic field. When the magnetic field is perpendicular to the light propagation, there is no linear magneto-optical effect. The case of a waveguide covered by magnetic metal is different. Inside of the metal the optical field is evanescent. As it will be shown below, in the case of evanescent field, the polarization rotates in xz-plane perpendicularly to the waveguide mode propagation direction (Fig. 11) even without magnetic field or anisotropy. Therefore, if the magnetic field

is applied perpendicularly to the waveguide mode propagation direction, since the polarization of the optical field is elliptical along this direction; there are MCD and Faraday effects. Both these effects contribute to the non-reciprocal loss.
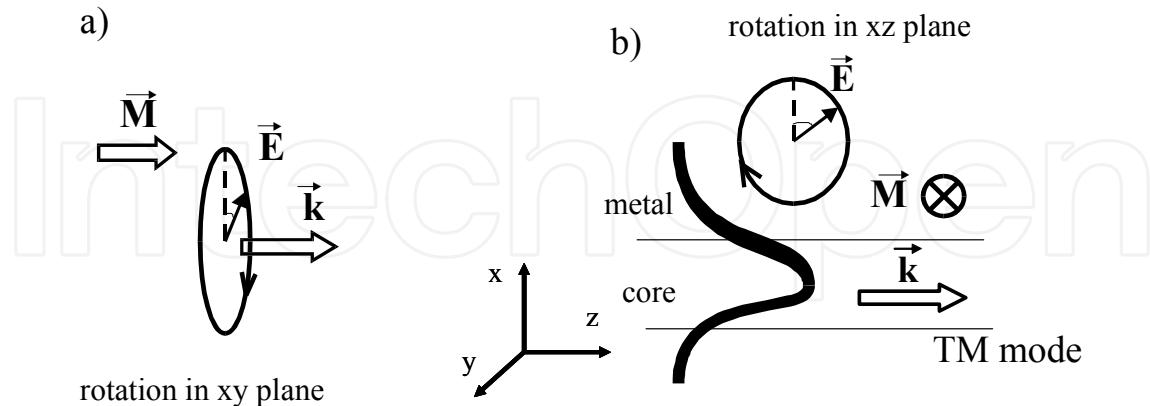

Fig. 11. Magneto-optical effect a) in bulk b) in waveguide covered by ferromagnetic metal.

The field of an electromagnetic wave is transverse. That means that the electrical field of the wave is always perpendicular to the wave vector. In the case of the light propagation in the bulk along z axis the electrical field can be described as

$$\vec{E} \sim e^{i(k_z z - \omega t)} + c.c. \quad \text{and} \quad E_z = 0 \tag{1}$$

For circular polarized wave, the polarization, which rotates in xy-plane, can be described as

$$\frac{E_x}{E_y} = \pm i \tag{2}$$

where + and – correspond to the right and left circular polarized waves.
Next, let us consider the waveguide covered by a magnetic metal. The electrical field in the metal can be described as

$$\vec{E} \sim e^{-k_x x + i(k_z z - \omega t)} + c.c. = e^{i(i k_x x + k_z z - \omega t)} + c.c \tag{3}$$

Since the electrical field of the electromagnetic wave is transverse $\vec{k} \perp \vec{E}$, for the TM mode ($E_y = 0$), we have

$$i k_x E_x + k_z E_z = 0 \quad \text{or}$$

$$\frac{E_x}{E_z} = i \frac{k_z}{k_x} \tag{4}$$

Comparing Eq. 4 and Eq. 2, it can be clearly seen that optical field in the metal is elliptically polarized and the polarization rotates in the xz-plane. Also, from Eq. (4) it can be seen that the ellipticity changes polarity for opposite directions of mode propagation (k_z -> -k_z). Therefore, if the magnetization of the metal is along the y-direction, the absorption will be different for two opposite mode propagation directions due to MCD effect. Also, the Faraday effect contributes to the non-reciprocal loss in waveguide. Due to the Faraday

effect the effective refractive index of the metal is different for the left and right circular polarizations. The absorption by the metal is directly proportional to the amount of light inside the metal and this in turn depends on the difference of refractive indexes between the metal and the waveguide core. If there is a change of refractive index due to the Faraday effect, it causes the change of optical absorption of waveguide mode by the metal.

The effect of non-reciprocal loss has another simple explanation. The propagation of waveguide mode can be considered as a plane wave, which propagates in the waveguide core and experiences multi reflections from boundaries of waveguide. If the magnetization of the metal is perpendicular to the plane of reflection, the plane wave experiences the transverse Kerr effect. The transverse Kerr effect states that if the reflection plane of the light is perpendicular to the magnetization of the metal, the absorption by the metal is different for two opposite directions of the magnetization. Therefore, the plane wave experiences different absorption for opposite propagation directions.

The optical isolation of the amplifier covered by ferromagnetic metal can be calculated by solving Maxwell's equations for multilayer structure. As an example of the waveguide isolator operating at a wavelength of 790 nm, we consider a $GaAs_{0.9}P_{0.1}/Al_{0.3}Ga_{0.7}As$ quantum-well (QW) optical amplifier covered by a Co layer (Fig. 12). To reduce the absorption by the Co layer, a buffer layer of p-$Al_{0.7}Ga_{0.3}As$ is inserted between the absorbing Co layer and $GaAs_{0.9}P_{0.1}/Al_{0.3}Ga_{0.7}As$ QW amplifying core layer. The optical field of a waveguide mode exponentially penetrates through the buffer layer into the Co layer.

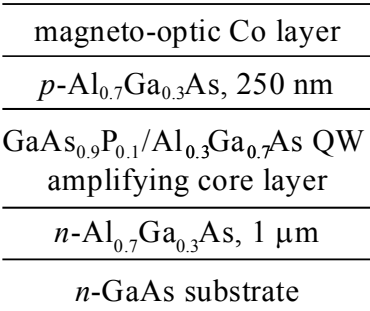| magneto-optic Co layer |
| --- |
| p-$Al_{0.7}Ga_{0.3}As$, 250 nm |
| $GaAs_{0.9}P_{0.1}/Al_{0.3}Ga_{0.7}As$ QW amplifying core layer |
| n-$Al_{0.7}Ga_{0.3}As$, 1 μm |
| n-GaAs substrate |

Fig. 12. GaAsP/AlGaAs optical amplifier covered by Co

Figure 13 shows the dependence of the optical loss/gain for the forward and backward propagating modes as a function of internal gain of the $GaAs_{0.9}P_{0.1}$ active layer. Depending
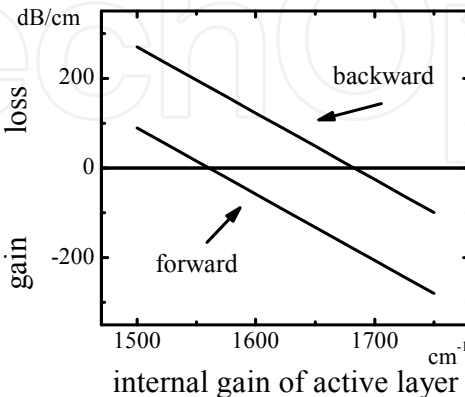

Fig. 13. Waveguide loss/gain as a function of the internal gain of $GaAs_{0.9}P_{0.1}$ active layer (Zaets&Ando, 1999).

on the value of the internal gain, the waveguide can operate as a non-reciprocal amplifier (internal gain >1680 cm-1) or as a non-reciprocal absorber (internal gain <1560 cm-1) or as an isolator (1560 cm-1> internal gain >1680 cm-1). The isolation ratio is almost constant against internal gain and it is about 180 dB/cm.

Because the waveguide mode interacts with the MO Co layer by its exponential tale through the buffer layer, the non-reciprocal loss/gain depends on the thickness of the buffer layer. Figure 14 shows a dependence of the isolation ratio and the internal gain of $GaAs_{0.9}P_{0.1}$ active layer as function of the thickness of the p-$Al_{0.7}Ga_{0.3}$ As buffer layer when the value of loss for the mode propagating in forward direction is kept to be zero. The thinner the buffer layer is, the larger isolation ratio can be obtained, although the higher amplification is necessary to compensate the loss.
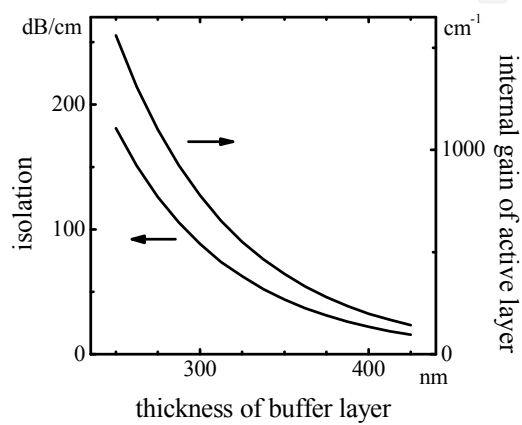
Fig. 14. Isolation ratio and the required internal gain of $GaAs_{0.9}P_{0.1}$ active layer vs. thickness of p-$Al_{0.7}Ga_{0.3}$As buffer layer. The loss/gain of the mode propagating in forward direction is fixed to be zero. (Zaets&Ando, 1999).

Figure 15 compares isolation ratio of structure of Fig.12 with Co, Fe and Ni cover layer. Wavelength dependence of optical constants of Co, Fe and Ni are taken into account, while
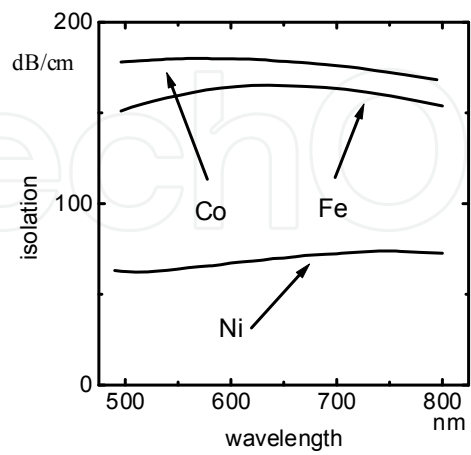
Fig. 15. Isolation ration vs. wavelength. Wavelength dependence of optical constants of Co, Fe and Ni are taken into account, while optical constants of amplifier is assumed to be independent on wavelength.

optical constants of amplifier are assumed to be independent of wavelength. Among these materials the cobalt is the most suitable for the proposed isolator. The isolation ratio only slightly changes vs. wavelength. Therefore, the wavelength dependence of the isolator is determined only by the bandwidth of the amplifier.

The proposed design of the isolator does not require the periodical reverse of magnetization or the phase matching between TE and TM modes or the interferometer structure. It provides the high isolation ratio in a wide range of the internal gain. The isolation ratio is proportional to the isolator length. These all merits make this design suitable for the monolithical integration of optical isolator with optoelectronic devices.

It should be noted that MO materials (ferromagnetic metals, magnetic semiconductors and magnetic garnets) show the highest values of the MO effect in a wavelength region where they show large absorption. Thus, the combination of the absorbing MO materials with the optical amplifiers is a viable way to achieve smaller sizes of non-reciprocal devices, which is suitable for integrated circuits.

For the experimental verification of the effect of non-reciprocal loss, we fabricated passive optical waveguides covered by a ferromagnetic metal. The directional dependence of absorption by the metal is a reason for the isolation in this structure. The optical gain in the isolator is used only to compensate the loss. To avoid side effects due to the optical amplification, we studied a passive waveguide covered by a ferromagnetic metal.

Two identical waveguides were fabricated, where only the material of buffer layer between Co layer and waveguide core was different. Figure 16(a) shows the structure of a $Ga_{1-x}Al_xAs$ waveguide covered by Co with SiO_2 buffer layer and Fig. 16 (b) shows the waveguide with AlGaAs buffer layer. The $Ga_{1-x}Al_xAs$ waveguide was grown with molecular-beam-epitaxy (MBE) on a GaAs (001) substrate. Following a 2500-nm-thick $Ga_{0.55}Al_{0.45}As$ clad layer and a 900-nm-thick $Ga_{0.7}Al_{0.3}As$ core layer, a buffer layer of 12-nm-thick SiO_2 or 120-nm-thick $Ga_{0.55}Al_{0.45}As$ was grown. The 10-μm-wide 600-nm-deep rib waveguide was wet etched. A 100 nm of Co layer and a 100 nm of Au layer were deposited on the buffer layer. A protection layer of 100-nm-thick SiO_2 with 8-μm-wide window was used to avoid light absorption at the sidewalls of the waveguide.
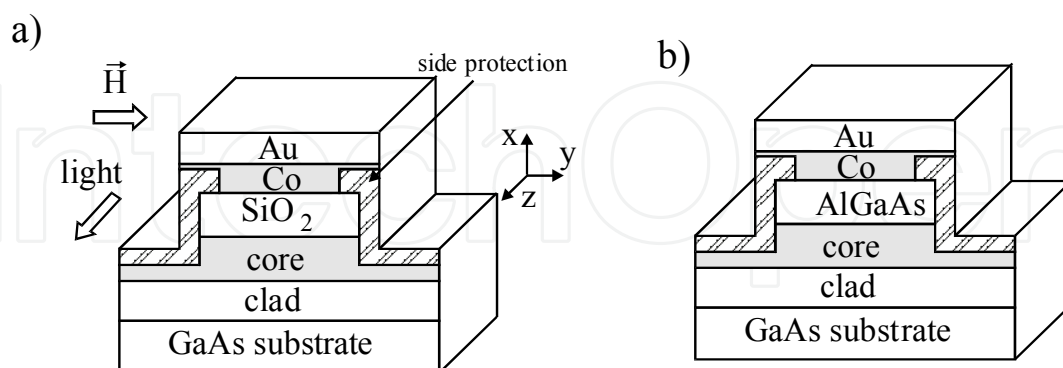

Fig. 16. AlGaAs optical waveguide covered with Co. Either a) SiO_2 or b) $Al_{0.45}Ga_{0.55}As$ was used as the buffer layer. Waveguide light propagates in the core layer and slightly penetrates into the Co layer.

For the evaluation of non-reciprocal loss, laser light (λ=770 nm) was coupled into the waveguide with a polarization-maintaining fiber. The output light was detected by a CCD camera. A polarizer was placed in front of the CCD camera. The magnetic field was applied

perpendicularly to the light propagation direction and in the film plane with an electromagnet.

Figure 17 shows the transmission coefficient of TM mode as a function of applied magnetic field for the waveguide with SiO_2 buffer and the waveguide with $Ga_{0.55}Al_{0.45}As$ buffer. A clear hysteresis loop of the transmission coefficient was observed with a coercive force of 35 Oe. The transmission coefficient of TE mode showed no dependence on the magnetic field. The magnetization curve measured by a superconducting quantum interface device (SQUID). For both samples magnetization curve was identical and the coercive force was 35 Oe. The observation of the hysteresis loop of the transmission coefficient of TM mode with the same coercive force is that of Co proves the TM mode transmission depends on magnetization of the Co. Considering time-inversion symmetry, the difference of transmission in the same direction of light propagation for two opposite directions of magnetic field is equal to the difference in transmission for opposite directions of light propagation in one direction of magnetic field. Therefore, the amplitude of the hysteresis loop of the transmission corresponds to the isolation provided by the waveguide. As can be seen from Fig. 17, the isolation direction for a waveguide with a SiO_2 buffer is different from that for a waveguide with a $Ga_{0.55}Al_{0.45}As$ buffer. Therefore, the isolation direction depends not only on the magnetization direction of the ferromagnetic metal, but on the waveguide structure as well.
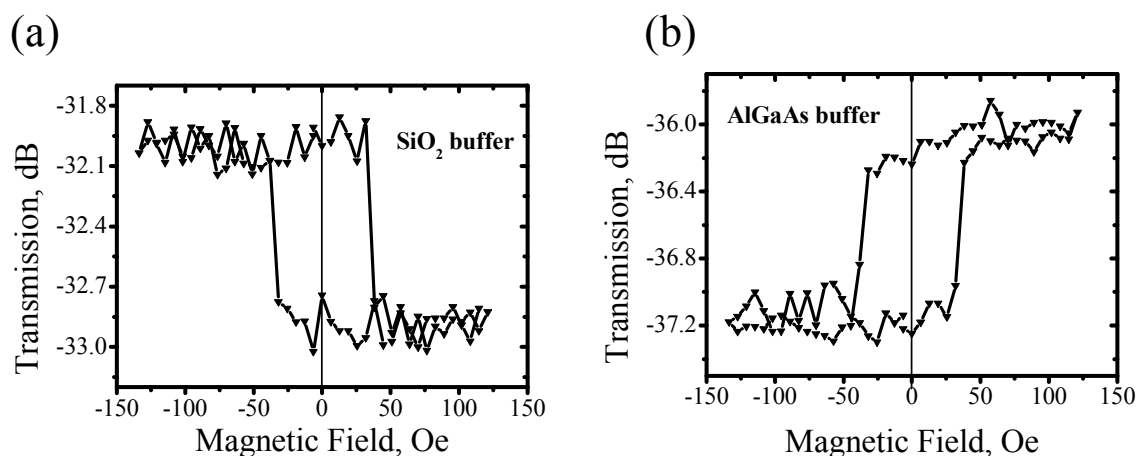

Fig. 17. Optical transmission in 1.1-mm-long $Ga_{1-x}Al_xAs$ optical waveguides covered by Co at λ=770 nm as a function of applied magnetic field a) with SiO_2 as the buffer layer and b) with $Ga_{0.55}Al_{0.45}As$ as the buffer layer. (Zayets &Ando (2005)).

These results can be explained by considering two contributions to the non-reciprocal loss by MCD and Faraday effects. We defined the figure-of-merit (FoM) for this isolator as a ratio of the non-reciprocal absorption to the total absorption by the metal. The mode propagation constants, non-reciprocal loss, and FoM were rigorously calculated from a direct solution of Maxwell's equations for the planar waveguide. In addition, both MCD and Faraday contributions to FoM were roughly estimated by estimating the light energy dissipation resulting from each contribution. For the waveguide with SiO_2 buffer, FoM was calculated to be 7.95%, where MCD and magneto-reflectivity contributions were estimated as -8.01 % and 15.86%, respectively. For the waveguide with $Ga_{0.55}Al_{0.45}As$ buffer, FoM was calculated to be -7.19%, where MCD and Faraday contributions were estimated as -8.01 % and 1.11 %,

respectively. The sign of the contributions is different. The magnitude of the MCD contribution is almost same for both waveguides. On the contrary, the magnitude of Faraday contribution is significantly different. That is a reason that opposite isolation directions were observed in the waveguides with SiO_2 and $Ga_{0.55}Al_{0.45}As$ buffers. For both waveguides the sums of the MCD and Farady contributions are approximately equal to the FoM calculated from the rigorous solution of Maxwell equations.

Next, we verify the isolation in the optical amplifier covered by the ferromagnetic layer. Figure 18 (a) showed the fabricated isolator. The optical amplifier consists of 8 $In_{0.46}Ga_{0.54}As/In_{0.26}Ga_{0.74}P$ tensile strained quantum wells grown on n-InP substrate. The p-InP was used as buffer layer and InGaAs as a contact layer. The amplifier has maximum amplification at λ=1566 nm. Figure 18 (b,c) shows the intensity of amplified spontaneous emission (ASE) as a function of applied magnetic field measured at both edges of the isolator, when the weak injection current of 10 mA was used. At each edge, a hysteresis loop was observed for ASE , however the polarity of the loop was different. It is because there is difference in gain for the light propagating in forward and backward directions in the amplifier.
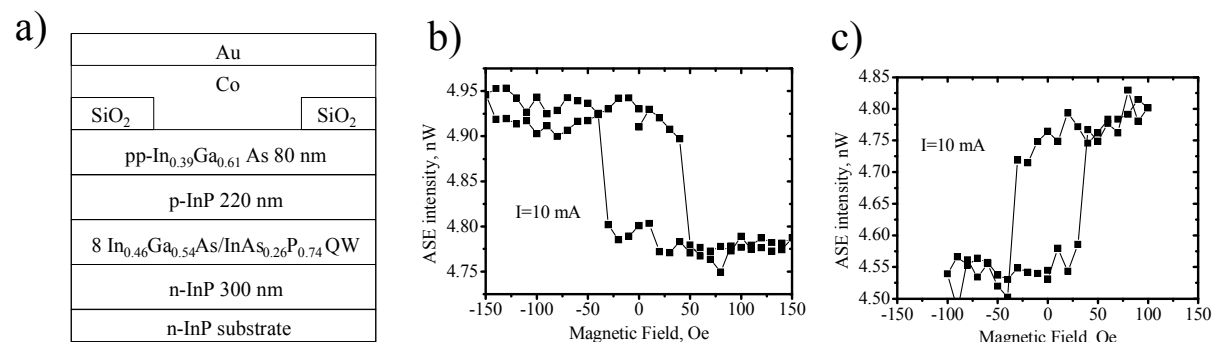

Fig. 18. a) InGaAs/InAsP optical amplifier with Co contact.Amplified spontaneous emission measured b)from left and c) right edge under small 10 mA injection current as a function of applied magnetic field.

Optical isolation of 147 dB/cm for TE mode was experimentally observed InGaAsP/InP optical amplifier at λ=1550 nm, in which one sidewall of waveguide was covered by TiO_2/Fe (Simizu & Nakano, 2004). Optical isolation of 147 dB/cm for TM mode at λ=1550 nm was reported for InGaAsP/InP covered by MnAs (Amemiya et al.,2007) and the optical isolation of 99 dB/cm for TM mode at λ=1300 nm was reported for AlGaInAs/InP optical amplifier covered by CoFe (Van Parys et al., 2006). In all these cases, to compensate the loss induced by the metal, the high injection current of more than 100 mA (current density more than 3 KA/cm²) is required. The required current is too high for the isolator to be used in practical devices. In order to be suitable for integration, the injection current for the isolator should be reduced. It is only possible if the figure-of-merit for non-reciprocal loss could be increased. As we showed above, there are two contributions into the non-reciprocal loss: Faraday effect and MCD. In the case of Fe or Co, these contributions have almost the same amplitude and opposite sign. The value of Faraday effect is roughly proportional to the real part of off-diagonal element of permittivity tensor of the metal and the value of MCD is roughly proportional to imaginary part of off-diagonal element. If some ferromagnetic metal could be found, for which mutual signs between imaginary and real part of off-diagonal

tensor element would be different to that of Fe and Co, it would make both contributions of the same sign and would significantly enlarge the figure-of-merit for the non-reciprocal loss.

4. Spin-photon memory

Photonics devices benefit from unique non-reciprocal properties of magneto-optical materials. If the material is ferromagnetic, the data can be stored in this material by means of two directions of residual magnetization. An ability to memorize data is another unique property of magneto-optical materials and it can be used for new designs of high-speed optical memory. Zayets & Ando (2009) proposed a new type of high-speed optical memory. Non-volatile data storage and high-speed operation are major advantages of this memory. Figure 19 shows the proposed design. The memory consists of micro-sized memory cells integrated on a semiconductor wafer. A bit of data is stored by each cell. Each cell consists of semiconductor-made photo detector and nanomagnet made of a ferromagnetic metal. The nanomagnet has two stable magnetization directions. The data is stored as a magnetized direction in the nanomagnet. For the data recording, the magnetization direction must be reversed by optical pulse. The circularly-polarized optical pulse is absorbed in the semiconductor detector creating spin-polarized electrons. Under applied voltage these spin polarized electrons are injected from the detector into the nanomagnet. The spin transfer torque is a consequence of the transfer of spin angular momentum from a spin-polarized current to the magnetic moment of a nanomagent. If the torque is sufficient, the magnetization turns and the data is memorized. Due to the optical selection rule, the spin-polarized electrons can be created only by the circular polarized optical pulse The linear polarized light excites equal amount of electrons of both up and down spins, therefore there is no net spin polarization, the current injected into nanomagnet is not spin polarized and there is no spin torque.
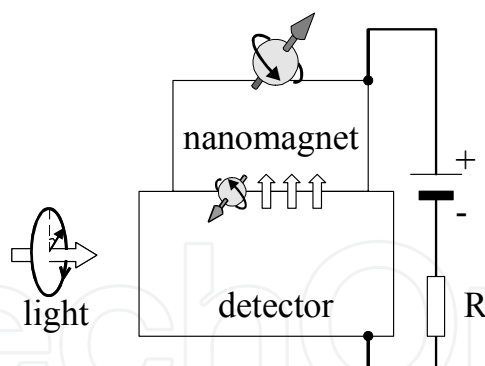

Fig. 19. Design of spin-photon memory. Zayets&Ando (2009)

Figure 20 shows integration of two memory cells and explains principle of high speed recording. There are two waveguide inputs. One input is for data pulses and one input is for the clock pulse. The clock pulse is used to select for recording a single pulse from sequence of the data pulses. Polarization of data pulses and clock pulse are linear and mutually orthogonal. Optical paths were split that each memory cell is illuminated by the data pulses and the clock pulse. The lengths of waveguides are adjusted so that the phase difference between clock and data pulses is $\lambda/4$ at each memory cell. At the first memory cell the clock pulse came at the same time with first data pulse. Therefore, these two pulses combined into one circularly polarized pulse. Since only first pulse is circularly polarized, only this pulse

excites spin polarized electrons, changes magnetization and is memorized. All other data pulses are linearly polarized, they do not excite spin polarized electrons and they have no effect on the magnetization. For the second memory cell, the clock pulse is slightly delayed relatively to the data pulses and it comes together with second data pulse. Only the second pulse is circularly polarized and can be memorized by the second memory cell. Therefore, each data pulse can be memorized by individual memory cell. The closer the pulses can be placed relatively to each other, the more data can be transformed through one line and the faster recording speed of memory can be achieved. The minimum interval between pulses, at which a pulse can be recorded without any influence of nearest pulse, determines the recording speed of the memory.
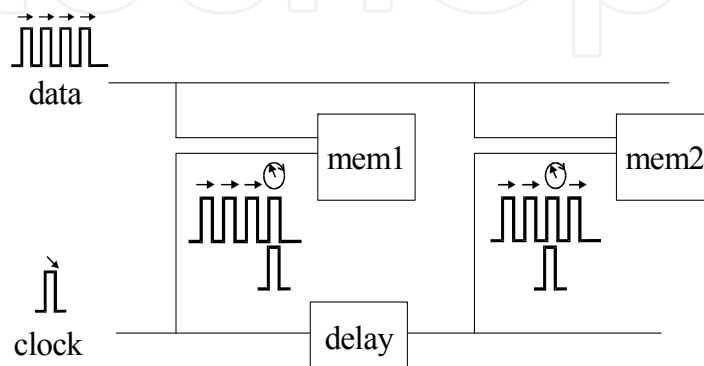
Fig. 20. The scheme for the integration of memory cells. Pulse diagrams explains the method for the high speed recording. Zayets & Ando (2009)

It was shown (Heberle et al., 1996) that spin-polarized excitons can by excited by two linearly cross-polarized pulses even the pulses arrived at different time. If the exciton dephasing time is longer than the interval between pulses, the excitons excited by two pulses can coherently interfere and create spin polarization.

For the successful demultiplexing by method proposed on Fig. 20, the interval between data pulses should be at least longer than electron dephasing time. Also, the spin polarization created by circularly polarized pulse should not be destroyed by following linear polarized pulses. Next, we verified the proposed demultiplexing method at the speed of 2.2 TBit/sec. For this purpose, we studied dynamics of excitation of spin polarized electrons in Si-doped GaAs (n=7x10^{16} cm-3) at 80° K.

Figure 21 shows the experimental setup. A mode-locked Ti:sapphire laser (λ=820 nm) provides 160 fs linearly-polarized pump and probe pulses. Polarization of the pump was rotated by a $\lambda/2$ waveplate and split by polarization beam splitter (PBS) into clock pulse and data pulse of linear and mutually orthogonal polarizations. The data pulse was split into two pulses. The second data pulse was 165 λ (~450 fs) delayed. Clock and data pulses were combined together by another PBS and focused on the sample. The linearly polarized probe beam was 100 ps delayed relatively to the pump and focused on the same spot on the sample. The spin polarization of electrons excited by pump beam was estimated from Kerr rotation angle of the probe beam. The rotation angle of reflected probe beam was measuring by polarizer (P) and photo detector (det). Intensity of each data pulse was 1-10 μJ/cm2. Intensity of the probe pulse was 10 times smaller. The data pulses and clock pulse were phase locked. When the clock pulse and one of data pulse nearly coincided, the positive and negative angles of Kerr rotation were observed for delays of (n+1/4)λ and (n-1/4)λ,

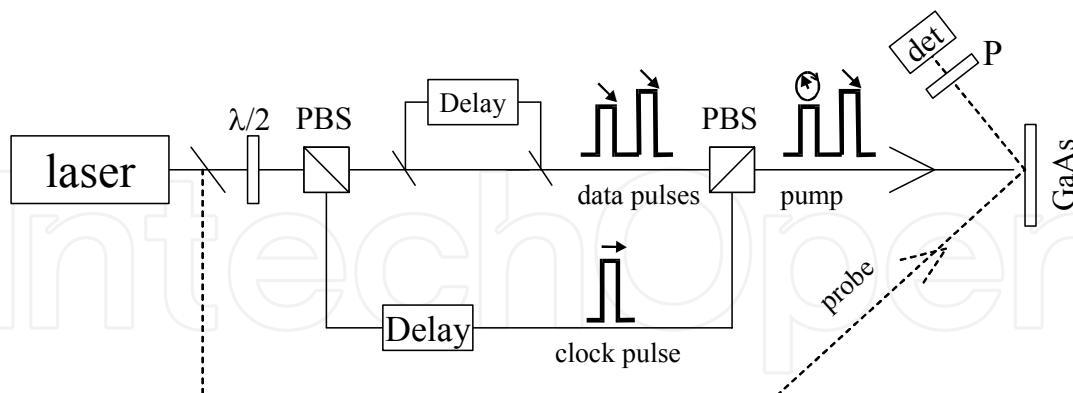respectively. When the pulses were away from each other, the Kerr rotation was not observed.

Fig. 21. Experimental setup for study the recording speed for spin-photon memory

Figure 22 shows spin polarization of the excited electrons as a function of delay between clock pulse and first data pulse. For each point the delay length was equal to $(n+1/4)\lambda$, where n is an integer. The maximum of spin polarization was observed when the clock pulse coincides with first data pulse. The spin polarization decreases when the clock pulse is delayed out of the first data pulse, and again increases as the clock pulse coincides with the second data pulse. Fig. 46 clearly shows that the spin polarization excited by the second data pulse can be separately distinguishable from the spin polarization excited by the first data pulse. This means that from two closely placed optical data pulses, only one pulse can trigger the recording without influence of another pulse. The interval between the data pulses is 450 fs. It corresponds to the recording speed of 2.2 TBit/sec. Notice that the detection of spin polarization was done 100 ps after data pulse arrived. This means that the lifetime of the spin polarized electrons is sufficient long to inject the spin polarized electrons into the nanomagnet for the magnetization reversal.
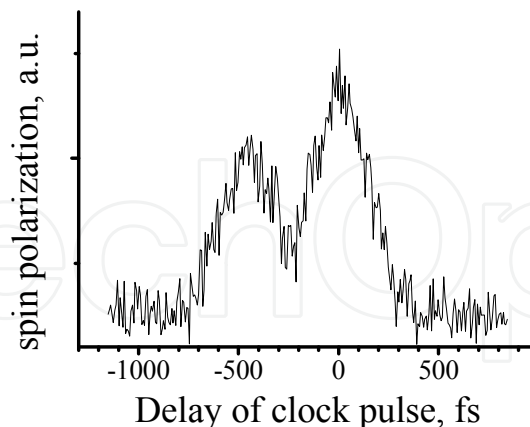

Fig. 22. Spin polarization of electrons excited by combined beam of clock pulse and two data pulse as a function of delay of clock pulse. For each point, the delay length was $(n+1/4)\lambda$, where n is integer. Reading of spin polarization was done 100 ps after arrival of pump pulses. Zayets & Ando (2009)

For the memory operating at speed 2.2 TBit/sec, the delay of clock pulse between cells (Fig. 21) should be $165 \cdot \lambda$ (~450 fs), the initial magnetization of all nanomagnets should be spin

down and the delay of data pulses relatively to the clock pulse should be $(1/4+m\cdot165)\cdot \lambda$, where m is a number of the data pulse. As result of Fig. 22, in this case in each cell only one data pulse excites spin polarization and memorized there. Other data pulses have no influence on spin polarization of that cell. In our experiment, the shortest interval between the data pulses, when the spin polarization excited by each pulse can be individually distinguished, is about 450 fs. For shorter interval the spin polarization is overlapped and the spin polarization created by preceding data pulse is reduced by next data pulse, which is causing overwriting of data of preceding pulse by next pulse in the cell. Therefore, the memory can not operate at speed faster than 2.2 TBit/sec.

By these experiments we demonstrated that from sequence of short-interval pulses it is possible to select only a single pulse for excitation of spin polarized electrons. That proves high recording speed of this memory. For the memory to be fully functional, the magnetization reversal by spin polarized photo-excited electrons should be realized. It requires injection of sufficient amount of spin-polarized current from detector into the nanomagnet (Slonczewski, 1996), Also, the time for the injection of the photo current from the detector into nanomagnet need to be adjusted so that it should be enough long to accomplish the magnetization reversal of the nanomagnet, but still it should be shorter than electron spin lifetime in the detector. The time, which takes for the magnetization of nanomagnet to turn between two stable direction, is about 500-1000 ps (Krivorotov, 2005). There are several semiconductors, in which the electron spin lifetime is longer or comparable with that time. For example, the spin life time is 100 ns in GaAs at T=4 K (Kikkawa & D. D. Awschalom, 1999) and 100 ps at room temperature (RT) (Hohage et al., 2006) 10 ns in GaAs/AlGaAs quantum well (QW) at RT (Adachi et al., 2001) and several ns in ZnSe QW at RT (Kikkawa et al.,1997). For the design of Fig. 19, the photo current injected in nanomagnet decays with time constant, where C is capacity of detector and R is resistance of close loop. The should be comparable with magnetization reversal time of the nanomagnet and smaller than the spin life time in the detector.

To estimate the energy of optical pulse required for magnetization reversal, we assumed that τ_{RC} is 500 ps, the efficiency of photon to spin conversion is 40 % and the critical current for the magnetization reversal is 5 mA (Kubota et al., 2005) To generate such current, the required energy of optical pulse should be about 3 pJ. It is in the range of the pulse energies which typically used in case of all-optical switching. Therefore, the memory may be suitable for the use in present optical communication systems.

Figure 23 shows the multiplexing scheme for this memory. For each memory cell, the optical waveguide passes under the nonomagnet. Due to the effect of non-reciprocal loss, the absorption of light in waveguide will be different for two opposite magnetization directions of the nanomagnet. The mode-locked laser, which could be integrated on the chip, provides the short pulses. The waveguide path is split, so that a pulse is split and it illuminates every memory cell. At output, all waveguide paths are combined. Each path has different length, so that each pulse reaches the output with a different delay and the amplitude of the pulse corresponded to the magnetization of each cell. Therefore, at the output the serial train of pulses will form with intensities proportional to the data stored in each memory cell.

This memory is compact, integratable, compatible with present semiconductor technology and it has fast operation speed. If realized, it will advance data processing and computing technology towards faster operation speed.
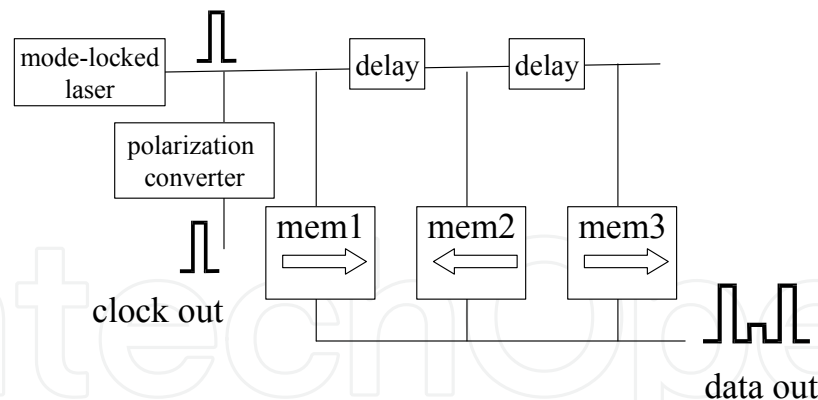
Fig. 23. Multiplexing scheme for spin-photon memory.

5. Conclusion

We have demonstrated that magneto-optical materials are important for optoelectronics, because of their unique non-reciprocal and memory properties. At present, there is an industrial demand for a waveguide-type optical isolator and a high-speed non-volatile optical memory. The use of magneto-optical materials is unavoidable for the fabrication of these devices.

6. Acknowledgement

7. References

T. Adachi, Y. Ohno, F. Matsukura, &H. Ohno (2001), " Spin relaxation in n-modulation doped GaAs/AlGaAs (1 1 0) quantum wells " *Physica E* vol. 10, 36-39, 2001.

T. Amemiya; H. Shimizu; M. Yokoyama; P. N. Hai, M. Tanaka & Y. Nakano (2007), " 1.54-μm TM-mode waveguide optical isolator based onthe nonreciprocal-loss phenomenon: device design to reduce insertion loss " *Applied Optics* vol. 46, No. 23, 5784 , Aug. 2007.

K. Ando; T. Okoshi, and N. Koshizuka, (1988) "Waveguide magneto-optic isolator fabricated by laser annealing," *Applied Physics Letters*, Vol. 53, 4-6 ,1988.

L.M. Augustin; R. Hanfoug, R.; J.J.G.J van der Tol,.; W.J.M de Laat & M.K Smit (2007) "A Compact Integrated Polarization Splitter/Converter in InGaAsP–InP", *IEEE Photonics Technology Letters* , Vol. 19, No. 17, 1286 – 1288, Sept. 2007 .

C. Brooks,P.E. Jessop, H. Deng , D.O. Yevick, G. Tarr (2006), "Passive silicon-on-insulator polarization-rotating waveguides ", *Optical Engineering* Vol. 45, No. 4, 044603, 2006.

M. C. Debnath; V. Zayets & K. Ando, (2007). "(Cd,Mn)Te/(Cd,Zn)Te quantum-well waveguide optical isolator with wide wavelength operational bandwidth" *Applied Physics Letters*, vol. 91, No.4, 043502 , July 2007.

H. Fukuda; K.Yamada,; T. Tsuchizawa; T. Watanabe;,H. Shinojima & S. Itabashi (2006) "Ultrasmall polarization splitter based on silicon wire waveguides" *Optics Express* Vol. 14, No. 25, 12401, Dec. 2006.

J. K. Furdyna (1988), "Diluted Magnetic Semiconductors," *Journal of Appled Physics* vol. 64, R29- R64, 1988.

A. P. Heberle; J. J. Baumberg; E. Binder; T. Kuhn; K. Kohler & K. Ploog (1996), "Coherent Control of Exciton Density and Spin" *IEEE Journal of Selected Topics in Quantum Electronics* vol. 2, No.3, 769-775 , Sep.1996.

P. E. Hohage, G. Bacher, D. Reuter & A. D. Wieck (2006), " Coherent spin oscillations in bulk GaAs at room temperature" *Applied Physics Letters,* vol. 89, No. 23, 231101, Dec. 2006.

J.Z. Huang, R. Scarmozzino, G. Nagy, M.J. Steel, R.M. Osgood (2000), "Realization of a compact and single-mode optical passive polarization converter ", *IEEE Photonics Technology Letters*, Vol. 12, No. 3, 317-319 , Mar 2000

J. M. Kikkawa & D. D. Awschalom (1999), " Resonant Spin Amplification in n-Type GaAs" *Physics Review Letters* vol. 80, No.19, 4313-4316, May 1999.

J. M. Kikkawa, I. P. Smorchkova, N. Samarth, & D. D. Awschalom (1997), " Room-Temperature Spin Memory in Two-Dimensional Electron Gases " *Science* 277, 1284-1287, Aug. 1997.

S.H. Kim, R. Takei, Y. Shoji & T. Mizumoto (2009) "Single-trench waveguide TE-TM mode converter ", OPTICS EXPRESS vol. 17, No. 14, 11267-11273. Jul.2009.

I. N. Krivorotov; N. C. Emley; J. C. Sankey; S. I. Kiselev D. C. Ralph & R. A. Buhrman (2005)," Time-Domain Measurements of Nanomagnet Dynamics Driven by Spin-Transfer Torques" *Science* vol. 307, 228-231, Jan. 2005.

H. Kubota; A. Fukushima; Y. Ootani; S. Yuasa; K. Ando; H. Maehara; K. Tsunekawa; D. D. Djayaprawira; N. Watanabe & Y. Suzuki (2005), " Evaluation of Spin-Transfer Switching in CoFeB/MgO/CoFeB Magnetic Tunnel Junctions " *Japanese Journal of Applied Physics* Vol. 44, No. 40, 2005, pp. L 1237–L 1240, Sep. 2005.

K. Onodera; T. Masumoto & M. Kimura (1994)" 980 nm compact optical isolators using Cd/sub 1-x-y/Mn/sub x/Hg/sub y/Te single crystals for high power pumping laser diodes," *Electronics Letters* Vol. 30, 1954- 1955, 1994.

J. C. Slonczewski (1996), "Current-driven excitation of magnetic multilayers" *Journal of Magnetism and Magnetic Materials* vol. 159, L1-L7, 1996.

H. Shimizu &Y. Nakano (2004), "First demonstration of TE mode nonreciprocal propagation in an InGaAsP_InP active waveguide for an integratable optical isolator," *Japanese Journal of Applied Physics* Part 2, vol. 43, L1561-L1563, Nov. 2004.

W. Van Parys,B. Moeyersoon, D. Van Thourhout, R. Baets, M. Vanwolleghem,B.Dagens, J. Decobert, O. Le Gouezigou, D. Make, R.Vanheertum & L. Lagae (2006), " Transverse magnetic mode nonreciprocal propagation in an amplifying AlGaInAs/InP optical waveguide isolator" *Applied Physics Letters,* vol.88, No.7, 071115, Feb. 2006.

H. Yokoi; T. Mizumoto; T. Takano & N. Shinjo (1999), "Demonstration of an optical isolator by use of a nonreciprocal phase shift," *Applied Optics* vol.38, 7409-7413, 1999.

W. Zaets; K. Watanabe & K. Ando (1997) "CdMnTe magneto-optical waveguide integrated on GaAs substrate," *Applied Physics Letters,* vol. 70, No. 19, 2508-2510, Mar. 1997.

W. Zaets & K. Ando (1999), "Optical waveguide isolator based on non-reciprocal loss/gain of amplifier covered by ferromagnetic layer", *IEEE Photonics Technology Letters* vol. 11, No.8, 1012-1014, Aug. 1999.

W. Zaets & K. Ando (2000), "Magneto-optical mode conversion in Cd1-xMnxTe waveguide on GaAs substrate," *Applied Physics Letters,* vol. 77, No. 11, 1593- 1595, Sep. 2000.

W. Zaets & K. Ando (2001), "Magnetically Programmable Bistable Laser Diode With Ferromagnetic Layer" *IEEE Photonics Technology Letters.* vol. 113, No.3, 185-187, Mar. 2001.

V. Zayets; M. C. Debnath & K. Ando (2004), "Complete magneto-optical waveguide mode conversion in Cd 1-xMnxTe waveguide on GaAs substrate," *Applied Physics Letters,* vol. 84, No. 4, 565- 567, Jan. 2004.

V.Zayets & K. Ando (2005), "Isolation effect in ferromagnetic-metal/semiconductor hybrid optical waveguide" *Applied Physics Letters ,* vol. 86, No. 26, 261105, June 2005.

V. Zayets & K.Ando (2009), "High-speed switching of spin polarization for proposed spin-photon memory" *Applied Physics Letters ,* vol. 94, vol.12, 121104 , Mar. 2009. Reprinted with permission from *American Institute of Physics* Copyright 2004, 2005, 2007, 2009 American Institute of Physics.
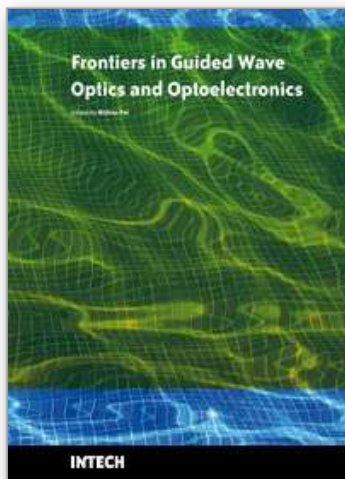
Frontiers in Guided Wave Optics and Optoelectronics

Edited by Bishnu Pal

As the editor, I feel extremely happy to present to the readers such a rich collection of chapters authored/co-authored by a large number of experts from around the world covering the broad field of guided wave optics and optoelectronics. Most of the chapters are state-of-the-art on respective topics or areas that are emerging. Several authors narrated technological challenges in a lucid manner, which was possible because of individual expertise of the authors in their own subject specialties. I have no doubt that this book will be useful to graduate students, teachers, researchers, and practicing engineers and technologists and that they would love to have it on their book shelves for ready reference at any time.

How to reference

In order to correctly reference this scholarly work, feel free to copy and paste the following:

Vadym Zayets and Koji Ando (2010). Magneto-Optical Devices for Optical Integrated Circuits, Frontiers in Guided Wave Optics and Optoelectronics, Bishnu Pal (Ed.), ISBN: 978-953-7619-82-4, InTech, Available from: http://www.intechopen.com/books/frontiers-in-guided-wave-optics-and-optoelectronics/magneto-optical-devices-for-optical-integrated-circuits

INTECH
open science | open minds